Brain Disorders 16 (2024) 100168

Contents lists available at ScienceDirect

Brain Disorders

journal homepage: www.sciencedirect.com/journal/brain-disorders

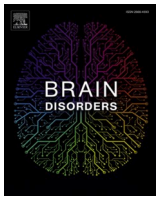

Platform for the radiomics analysis of brain regions: The case of Alzheimer's disease and metabolic imaging

Ramin Rasi, Albert Guvenis, for the Alzheimer's Disease Neuroimaging Initiative[1]

Institute of Biomedical Engineering Boğaziçi University, Turkey

ARTICLE INFO

Keywords:
Alzheimer's disease (AD)
Mild cognitive impairment (MCI)
FDG PET
Machine learning
Radiomics

ABSTRACT

Objective: This study introduces a PET-based platform for brain radiomics analysis. We automatically identify key brain regions and features associated with Alzheimer's disease (AD), enabling more accurate diagnosis and staging compared to using predefined regions.
Methods: To create an integrated platform that covers all the phases of radiomics, we obtained FDG-PET images of 549 individuals from the ADNI database. We used FastSurfer to segment the brain into 95 regions. We then obtained 120 features for each of the 95 ROIs. We employed eight feature selection methods to select and analyze the features. We finally utilized nine different classifiers on the 20 most significant features extracted.
Results: For all three predictions AD vs. cognitively normal (CN), AD vs. mild cognitive impairments (MCI), and CN vs. MCI the Random Forest (RF) classifier with LASSO demonstrated the highest accuracy with an AUC of 0.976 for AD vs CN, AUC=0.917 for AD vs MCI, and AUC=0.877 for MCI vs CN. This is the highest performance that we encountered compared to the studies in the literature. Three subregions hippocampus, entorhinal, and amygdala could then be identified as critical.
Conclusion: A brain radiomics platform can enable an efficient, standardized, and optimally accurate AD and MCI diagnosis from FDG PET images by using an automated pipeline. The three regions identified as having the highest discriminating power confirm the findings of previous clinical research results on AD. While the focus was AD in this study, the platform can potentially be used to address other brain conditions.

1. Introduction

Alzheimer's disease (AD), the most common progressive neurological disease among elderly individuals, is a neuropsychiatric disorder that causes many economic and psychological difficulties for the patient's community and family[1]. According to the estimation of the World Health Organization (WHO), the number of people with age over 60 years old will reach 2.1 billion people by 2050[2]. In a study, researchers show that Alzheimer's disease starts building up in the brain long before symptoms appear[3], and therefore it is possible to detect this pathology in vivo using biomarkers such as molecular imaging techniques in the early stage of formation[4]. Given the intricate nature of AD as a gradual, multifaceted ailment, healthcare professionals employ an array of clinical assessments and neuroimaging methods in their work to detect dementia during its early phases[5,6]. These techniques not only enhance the ability to detect diseases at their early stages but also facilitate the delineation of novel therapeutic strategies that are customized to individual patients[7].

A number of studies are available in the literature that aim to detect AD and its stages using computational methods and molecular imaging modalities such as Positron Emission Tomography. Here we present a few significant and recent studies. A more comprehensive summary in the form of a table is given in the discussion section.

A pivotal study[8] leveraged two distinct imaging techniques, Fluorodeoxyglucose (FDG) PET and MRI, to predict the presence of MCI or AD. Their results were quite promising, achieving an impressive AUC of 0.98 for distinguishing AD from CN and an AUC of 0.85 for discerning MCI from CN. The study employed the LASSO feature selection on characteristics extracted from the hippocampus and utilized a logistic regression model with cross-validation (CV=5).

In a meta-analysis study[9], researchers investigated the potential of machine learning (ML) algorithms to aid in the automated detection and

E-mail addresses: Raminrasi@yahoo.com (R. Rasi), guvenis@boun.edu.tr (A. Guvenis).

[1] Data used in preparation of this article were obtained from the Alzheimer's Disease Neuroimaging Initiative (ADNI) database (adni.loni.usc.edu). As such, the investigators within the ADNI contributed to the design and implementation of ADNI and/or provided data but did not participate in the analysis or writing of this report. A complete listing of ADNI investigators can be found at: http://adni.loni.usc.edu/wp-content/uploads/how_to_apply/ADNI_Acknowledgement_List.pdf

https://doi.org/10.1016/j.dscb.2024.100168

Available online 16 October 2024

Table 1
Clinical characteristics of participants.

Clinical Diagnosis	No. Cases	Sex (M/F)	Age (mean ± SD)
AD	163	91/72	74.6 ± 8.12
MCI	198	107/91	72.5 ± 8.07
CN	188	91/97	73.6 ± 6.37
Total	549	289/260	74.1 ± 7.02

diagnosis of diseases, with a special focus on the detection of Alzheimer's disease using medical imaging as a non-invasive biomarker. Their analysis encompassed 24 distinct ML models from 19 research papers, covering various brain regions. The highest achieved AUC was 0.93. The study also highlights the prevalence of internal validation as a limitation in the field, a concern raised in another study [10], where only 6 % of the 516 reviewed studies utilized external validation. This meta-analysis underscores the encouraging performance of ML in diagnosing AD, while also emphasizing the need for high-quality, large-scale prospective studies to enhance its reliability and applicability in clinical practice.

Another investigation[11], proposed a model to predict the progression of MCI to AD using FDG PET images. This study focused on white matter and constructed an integrated model, applying it to features extracted from this region. The research revealed the association of white matter with MCI progression to AD and highlighted differences between two groups of patients with stable and progressing MCI. FDG PET was found to significantly improve the prediction of MCI to AD progression compared to MRI and cerebrospinal fluid analysis[12]. This study opted for FDG PET due to its cost-effectiveness and ease of implementation in contrast to other radiotracers used to measure TAU and Amyloid proteins. Furthermore, the study combined FDG PET features with clinical data to identify high-risk MCI patients.

These studies often employed predefined regions based on domain knowledge and rely on specific regions' uptake values as mentioned above, necessitating tools such as SPM for analysis. While these tools provide interpretable results by calculating uptake ratios in specific regions, the limited selected number of features may not be optimal. Furthermore, the lack of a specific hardware/software platform may require longer computational and man-machine interaction times.

The development of advanced radiomics methods and special platforms for their efficient and standardized implementation has recently gained momentum for a number of applications, in particular in oncology.

Radiomic analysis is an emerging area that has been developed to discover imaging biomarkers for characterizing diseases. This technique permits the prediction of various characteristics such as prognosis, stage, type, and therapy response using a very large number of imaging features. These features are then reduced to improve the efficiency, performance, and interpretability of machine learning models[13]. Furthermore, the significant image regions of interest and features can be used to help explain the examined pathology. If no predetermined regions and features are used, our hypothesis is that the final model incorporating the optimally reduced set of features may potentially yield a higher accuracy compared to methods that use assumptions based on domain knowledge. Since radiomics is very computationally intensive and requires standard algorithms, it may also help to use a special-purpose hardware and software platform. Radimics has been applied to oncology in particular but lately, other applications started to gain momentum including those addressing AD[14–16].

A few studies[17,18] have been conducted to develop special hardware and software platforms for radiomics analysis. This facilitates the task and makes the computation more efficient, automatic, reproducible, and user-friendly.

In a recent study[19], researchers introduced a web-based tool named RayPlus. This tool has been specifically developed for conducting texture analysis on images from CT, MRI, and PET scans. RayPlus stands out by providing histogram analysis, which furnishes a clear and intuitive representation of the delineated Region of Interest (ROI/VOI). Its purpose is to analyze medical images comprehensively, without a specific focus on any particular anatomy or disease.

In another study[20] researchers have devised a platform for the analysis of CT images. This platform encompasses all the stages of the radiomics process, including labeling, feature extraction, feature selection, classifier training, and statistical result visualization. An interesting feature of this platform is its utilization of both semi-automatic and fully automatic segmentation techniques for labeling ROIs. This versatile platform is implemented as a general and open-source software package, employing the Python programming language.

These platforms present limitations however, owing to their reliance on manual or semi-automatic delineation algorithms, a lack of specific focus on particular anatomies or diseases, and challenges in seamless integration with emerging hardware configurations. The significant challenge of intra- and interobserver variability in radiomics workflows due to semi-automatic delineation methods is evident. The platforms' inability to smoothly integrate with evolving hardware configurations, such as Graphics Processing Units (GPUs), hinders their ability to optimize computational efficiency. These constraints underscore the need for developing more dynamic and adaptable radiomics platforms for specific purposes.

In this study, we tried to overcome the above-mentioned limitations by using a new specialized brain radiomics platform and determining the few ROIs and features that may help explain the results.

In particular, we present a new radiomics platform for specifically brain PET studies. In order to streamline and mechanize the procedure, we have integrated a software module into our workflow for volumetric analysis and automated segmentation of the brain into a large number of regions using an atlas[21].

In order to demonstrate the benefits of such a platform, we conducted a test study using FDG PET images in order i) To enable the early accurate and efficient detection of AD from FDG PET images ii) To identify the few regions and features that explain the pathogenesis of AD and iii) To distinguish between the different stages of AD. This study is different from most previous radiomics work[22] in the area of AD since no brain regions are pre-assumed and therefore the optimal few brain regions identifying the different AD stages are found automatically. This also gives a way to develop an explanation of the AD pathogenesis based on the meaning of the obtained set of features and improve interpretability.

2. Method

Our methodology involves systematic steps, depicted in Fig. 1, beginning with pre-preprocessing and labeling the data. Then extract regions of interest (ROIs) using FastSurfer. Feature extraction follows, where we compute 120 features from FDG PET images. These features underpin our radiomics analysis for early diagnosis and interpretation. Subsequent sections delve into each step's details.

2.1. ADNI and participants

Data used in the preparation of this article were obtained from the Alzheimer's Disease Neuroimaging Initiative (ADNI) database (adni.loni.usc.edu). The ADNI was launched in 2003 as a public-private partnership, led by Principal Investigator Michael W. Weiner, MD. The primary goal of ADNI has been to test whether serial magnetic resonance imaging (MRI), positron emission tomography (PET), other biological markers, and clinical and neuropsychological assessment can be combined to measure the progression of MCI and early Alzheimer's disease. Detailed information about the participants' clinical characteristics can be found in Table 1.

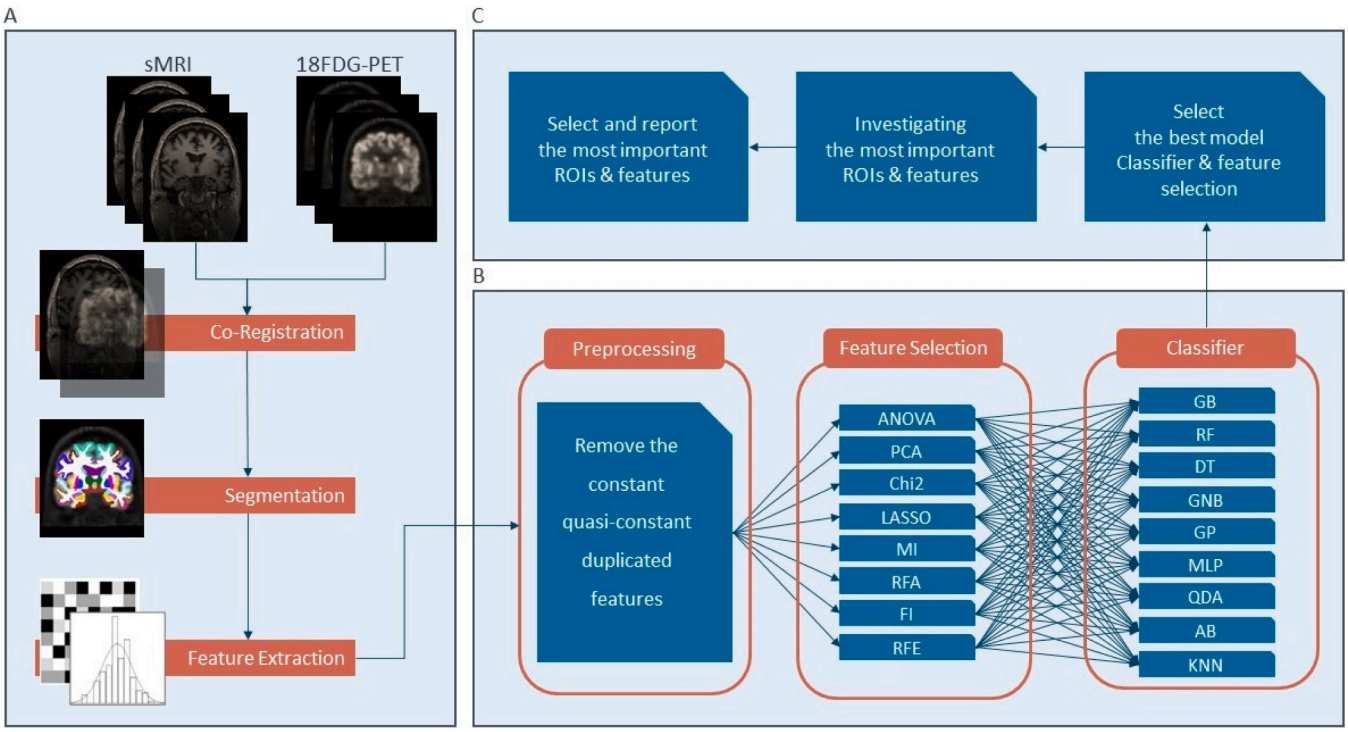

Fig. 1. Illustrates a comprehensive view of the proposed method. (A) The initial stage encompasses segmentation and feature extraction. (B) In the model-building phase, dimension reduction and classification steps are undertaken. (C) The analysis phase involves choosing the optimal model and scrutinizing features and regions of the brain.

2.2. PET Acquisition

The 18-fluoro-deoxyglucose PET imaging data, obtained during the initial visit to the ADNI database, were furnished in two forms: raw and preprocessed, and then categorized into four distinct groups based on the applied preprocessing procedures, as detailed on adni.loni.usc.edu. These data consisted of dynamic 3D scans, with a radiotracer dosage of 185 MBq (5 mCi), comprising six 5-minute frames captured between 30 and 60 min post-injection. For our analysis, we specifically utilized the third type of preprocessed FDG PET image data, characterized by Co-Reg, AVG, Standardized Image, and Voxel Size adjustments. Within this dataset, the FDG PET images were adjusted to adhere to a standardized 160×160×96 voxel imaging grid, with each voxel measuring 1.5 mm on all sides, as referenced in[23]

2.3. ROI Extraction

The Volumetric Segmentation component of FastSurfer, a deep learning-based method, was employed to expedite the anatomical segmentation process. This tool operates on coronal, axial, and sagittal 2D slice stacks, leveraging local and global competition within its F-CNNs. The integration of multi-slice information aggregation and competitive dense blocks enhances the network's ability to accurately recognize both cortical and sub-cortical structures. FastSurfer's efficiency and speed in handling large datasets significantly streamline the analysis process, enabling the swift and precise segmentation of the entire brain into 95 regions, a crucial step for our radiomics approach.

2.4. Feature Extraction

To extract the features from FDG PET, we used an open-source Python package: PyRadiomics[24]. We calculated 120 feature classes: first-order statistics (19), gray level dependence matrix (14), shape-based (2D) (10), gray level cooccurrence matrix (24), gray level run length matrix (16), neighboring gray-tone difference matrix (5), gray level size zone matrix (16 features) and shape-based (3D) (16). All features were computed from the extracted 95 ROIs in FDG PET images.

2.5. Feature Selection

In the realm of radiomics research, feature selection is crucial for condensing the extensive array of features derived from available datasets[25,26] and for improving performance. Our evaluation encompassed a comprehensive study of the effectiveness of various feature selection techniques, including filtered, embedded, wrapper, and hybrid methods, each holding their distinct advantages[27]. To ensure the robustness of our approach, we opted for widely used algorithms from each category[28–30]. These encompassed ANOVA, PCA, chi-square, LASSO, MI, RFA, FI, and RFE among others[31], all carefully considered to identify the most pertinent subset of features for our radiomics analysis.

2.6. Classification and tuning

Researchers have developed a range of classification methods[32] and identifying the most suitable machine-learning approach for radiomics applications is a pivotal phase, with high-performing classifiers contributing significantly to the enhancement of clinical applications based on radiomics. In our investigation, we assessed the performance of nine classification methods, spanning various classifier families, including GradientBoosting (GB), RandomForest (RF), DecisionTree (DT), GaussianNB (GNB), GaussianProcess (GP), MLP, QuadraticDiscriminantAnalysis (QDA), AdaBoost (AB), and KNeighbors (KNN), in conjunction with eight different feature selection techniques. This exhaustive analysis, resulting in 72 distinct combinations of classification methods and feature selection methods, led to the selection of classifiers that exhibited the most favorable area under the ROC curve for our proposed solution. This selection process was executed with default parameters as stipulated in the Scikit-learn library, and we also paid close attention to the critical task of hyperparameter optimization.

To achieve this, we conducted randomized search cross-validation (CV=5) tuning using 70 % of the data, reserving 30 % for independent testing, and iterated this process 100 times under completely random conditions[33,34].

2.7. Evaluation Metrics

To evaluate the performance of the nine classifiers comprehensively, we initially employed the Receiver Operating Characteristic (ROC) curve analysis. Given the critical nature of accurate medical diagnosis, ROC AUC, a robust metric that measures a model's ability to distinguish between positive and negative instances, was selected as the primary evaluation criterion. This choice allowed for a direct comparison of the classifiers' performance without being influenced by class imbalance. Following the selection of the optimal classifier, a more detailed evaluation was conducted using additional metrics: Accuracy, Specificity, and Sensitivity. By incorporating these metrics, we obtained a well-rounded understanding of the classifier's performance in terms of both overall accuracy and its ability to correctly classify both positive and negative instances.

2.8. Design of rab-pet

The deployment of the RAB-PET platform was dedicated to addressing two principal challenges. Initially, there was a concerted effort to utilize parallelized methods, aiming to expedite the processing time across different steps in our prediction utilizing radiomics approaches. This initiative proved successful, reducing the processing time to under 70 s. The second major focus was creating an integrated platform that covers all phases of radiomics, including segmentation, feature extraction, and prediction. This platform stands as a groundbreaking endeavor, marking the first integrated system specifically designed to predict and analyze Alzheimer's disease.

2.9. Computational hardware and software

The computational methodology delineated in this investigation incorporates a sequential approach for the early detection and interpretation of AD through the utilization of FDG PET imaging data. The architecture of the RAB-PET software, crafted on Linux Ubuntu 22.04 LTS and employing Python 3.10.13, integrates pivotal components such as ANTs and FastSurfer for co-registration and segmentation. Furthermore, our platform leverages the PyRadiomics component to parallelize the computation of feature values under ISBI [35,36]. The integration of Python and PyTorch augments the computational capabilities of the platform, making use of CUDA technology to harness parallel processing. The hardware framework supporting the RAB-PET platform encompasses a Core i7 Gen10th processor, 16 GB DDR5 RAM, an RTX2060 VGA card featuring 1920 CUDA cores, and 240 Tensor Cores capable of delivering 52 teraflops of deep learning power, particularly instrumental in the segmentation step. The code for the prediction model can be found in the Zendo data repository[37].

3. Results

In this research, we conducted predictions in three distinct categories: AD and CN, MCI and CN, and MCI and AD. To perform these predictions, we independently evaluated each of these three predictions using a substantial number of features extracted during the initial stage, totaling 11,400 features for each image (120×95). It's crucial to note that having an excessive number of features can lead to overfitting, which is a common challenge in supervised machine learning[38]. To mitigate this issue, we employed feature reduction techniques aimed at reducing the feature count. The selection of an appropriate algorithm for feature reduction is a critical decision in the field of machine learning, as highlighted in the reference[39]. Before applying the feature reduction methods to our extracted features, we first preprocessed these features. This preprocessing involved eliminating constant, quasi-constant, and duplicated features. This step is essential for ensuring the quality of the feature set. With our preprocessed feature set, consisting of 5351 features, we embarked on a comprehensive exploration of various dimension reduction methods to identify the most effective approach for our problem. Subsequently, we calculated the accuracy of each subset of the most significant features using a rank-based method. Throughout this comparison, we adhered to the default parameters as defined in the Scikit-learn library for all classifiers. We refrained from hyperparameter tuning, as our primary focus was on the feature reduction aspect of the machine learning process.

3.1. AD vs cn

The outcomes displayed in Table 2 reveal that among the various classifiers and feature selection methods evaluated, the Random Forest (RF) classifier with LASSO exhibited the most impressive performance, achieving a good accuracy with an Area Under the Curve (AUC) value of 0.976. This accuracy surpassed the performance of all other combinations of classifiers and feature selection techniques, underscoring the superiority of the RF classifier when applied to features selected via the LASSO method. This finding highlights the effectiveness of this specific combination in achieving high-quality results in our study.

Based on the data presented in Table 2, it's evident that the Random Forest (RF) classifier outperformed other classifiers and feature selection methods in terms of accuracy, achieving an impressive AUC of 0.976. This level of accuracy was notably higher than what was attained with alternative combinations of classifiers and feature selection techniques. To reach this result, we followed a specific process.

First, we preprocessed all extracted features (n = 11,400) by removing constant, quasi-constant, and duplicated features and reducing them to 5351. Next, we applied the LASSO method to the preprocessed feature set. Subsequently, we utilized a rank-based method, which leveraged the coefficients of the features, to calculate the average accuracy across all subsets of the selected top 20 features by LASSO. This calculation was performed through 100 iterations for each subset, using 30 % independent test data.

The RF classifier, when applied to features obtained via the LASSO algorithm and subjected to 100 iterations, demonstrated a high area under the curve (AUC) of 0.976, with a 95 % confidence interval ranging from 0.95 to 0.98. This signifies the robustness and reliability of the RF classifier when working with these features of the LASSO method.

Fig. 2 provides a graphical representation of our findings. It illustrates that after including four features, there is minimal improvement in performance. These four Regions of Interest (ROIs) are the isthmus cingulate (left hemisphere), inferior parietal (left hemisphere), hippocampus (left hemisphere), and entorhinal (right hemisphere). The selected features consist of first-order 90Percentile, first-order Median, glrlm LongRunEmphasis, and gldm DependenceEntropy.

Furthermore, leveraging the four most crucial features, as depicted in Table 5, we evaluated the performance of the tuned classifier. Upon selecting the RF classification method and fine-tuning its hyperparameters using randomized-search cross-validation (with a 5-fold cross-validation), we achieved an AUC of 0.961 with 100 iterations and a 95 % confidence interval spanning from 0.938 to 0.982. These results, coupled with an accuracy of 0.91, sensitivity of 0.89, and specificity of 0.92, further underscore the efficacy of the RF classifier in producing consistent and high-quality results for our classification model.

3.2. AD vs MCI

In the context of distinguishing between AD and MCI, our analysis revealed that the Random Forest (RF) classifier, when applied to features selected through the LASSO method, delivered the highest level of

Table 2
(Heatmap) Results of performing nine classifiers GB, RF, DT, GNB, GP, MLP, QDA, AB, and KNN on the top 20 features selected by eight dimension-reduction methods ANOVA, PCA, Chi-Square, LASSO, MI, RFA, FI, and RFE.

`	GB	RF	DT	GNB	GP	MLP	QDA	AB	KNN
ANOVA	0.957	0.962	0.85	0.961	0.91	0.935	0.958	0.951	0.912
PCA	0.92	0.929	0.784	0.919	0.677	0.853	0.918	0.904	0.79
Chi Square	0.936	0.941	0.825	0.947	0.934	0.928	0.942	0.918	0.919
LASSO	0.971	0.976	0.874	0.971	0.914	0.919	0.972	0.967	0.909
MI	0.952	0.951	0.838	0.947	0.906	0.916	0.94	0.939	0.903
RFA	0.968	0.968	0.872	0.97	0.942	0.897	0.966	0.955	0.919
FI	0.949	0.955	0.838	0.955	0.92	0.941	0.952	0.933	0.921
RFE	0.959	0.964	0.853	0.965	0.899	0.939	0.955	0.943	0.927

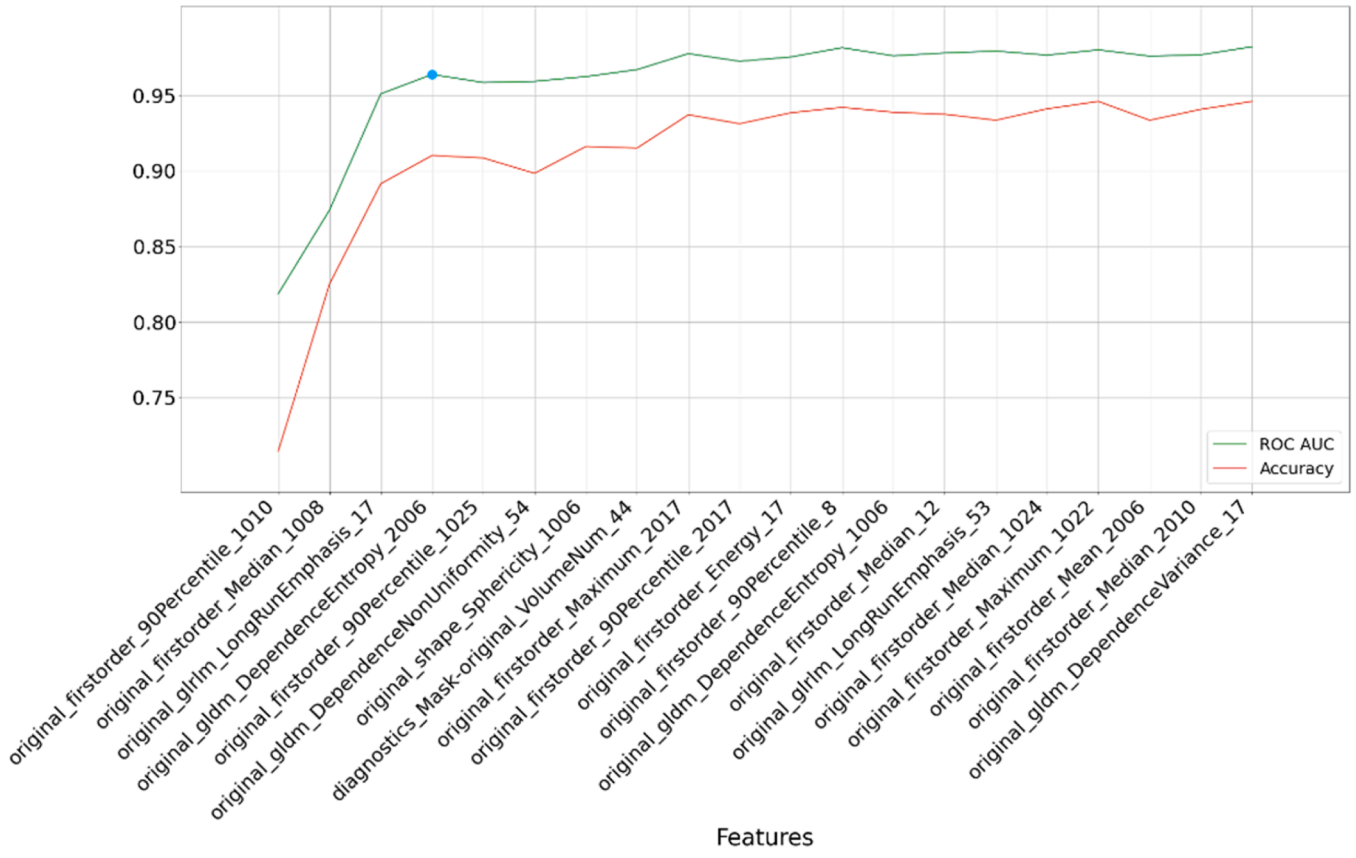

Fig. 2. Rank-based results for each subset of the top 20 most important features selected by the LASSO method. The blue point is the optimal point based on accuracy and feature count. The numbers at the end of the feature names correspond to the ROI IDs provided by Fastsurfer.

Table 3
(Heatmap) Results of performing nine classifiers GB, RF, DT, GNB, GP, MLP, QDA, AB, and KNN on the top 50 features selected by the eight dimension-reduction methods ANOVA, PCA, Chi2, LASSO, MI, RFA, FI, and RFE to predict AD vs MCI.

`	GB	RF	DT	GNB	GP	MLP	QDA	AB	KNN
ANOVA	0.815	0.815	0.683	0.843	0.772	0.806	0.818	0.787	0.781
PCA	0.758	0.782	0.625	0.796	0.615	0.744	0.777	0.751	0.693
Chi Square	0.781	0.813	0.668	0.83	0.836	0.812	0.804	0.768	0.796
LASSO	0.862	0.917	0.72	0.889	0.787	0.825	0.857	0.825	0.748
MI	0.843	0.837	0.698	0.828	0.793	0.798	0.815	0.826	0.793
RFA	0.872	0.862	0.724	0.871	0.791	0.799	0.845	0.851	0.782
FI	0.863	0.868	0.716	0.852	0.778	0.822	0.823	0.833	0.77
RFE	0.834	0.829	0.693	0.835	0.798	0.797	0.804	0.805	0.763

accuracy. This achievement is shown in Table 3, where the classifier yielded an AUC of 0.917.

Further refinement of our analysis led us to identify the most critical features—six in total—based on their impact on accuracy, as illustrated in Fig. 3. Even with this more concise feature set, the model exhibited commendable accuracy, resulting in an AUC of 0.862, as depicted in Table 5.

To carry out this prediction task for AD vs MCI, we initially applied LASSO to a preprocessed feature set, containing 5351 features. Subsequently, we employed a rank-based approach, focusing on the top 50

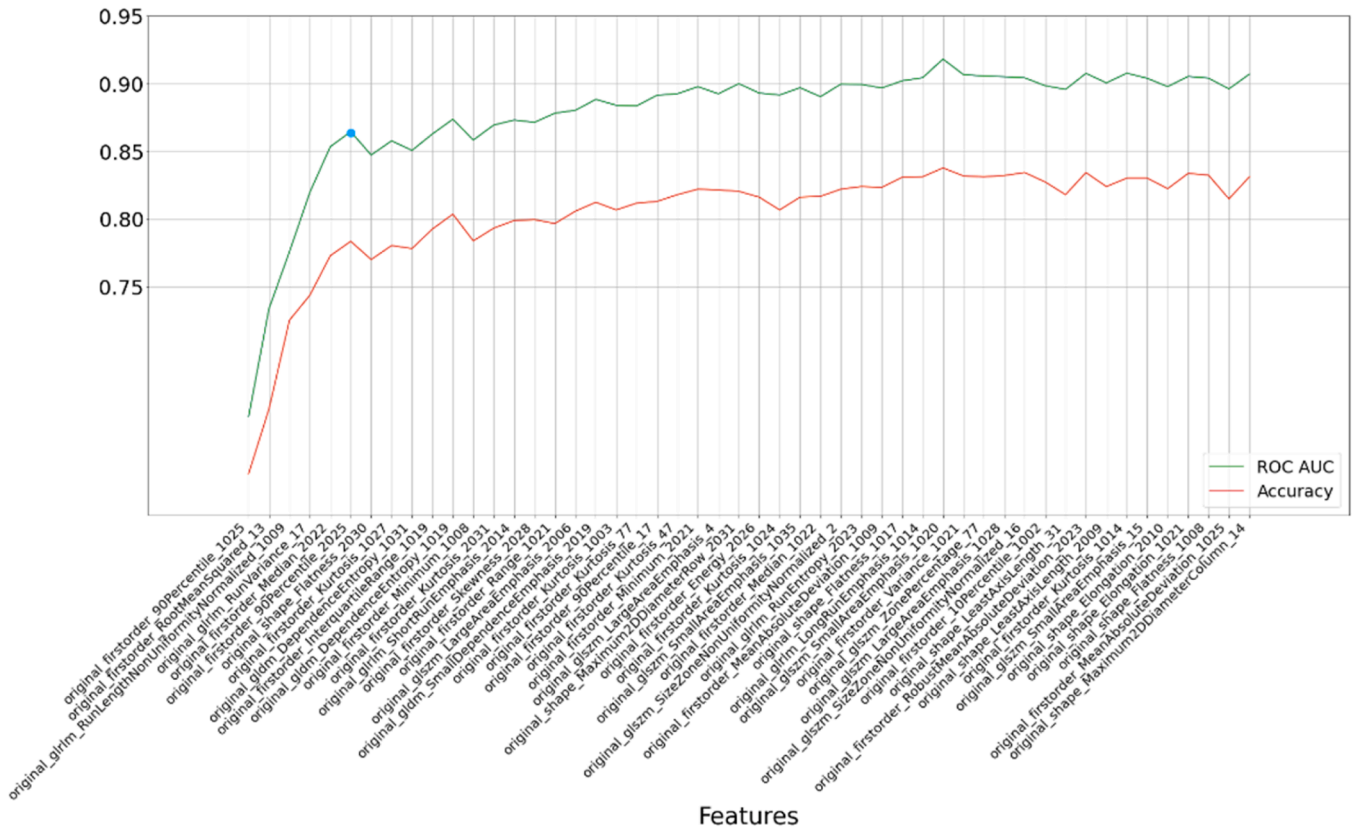

Fig. 3. Rank-based results for each subset of the top 50 most important features selected by the LASSO method. The blue point is the optimal point based on accuracy and feature count. The numbers at the end of the feature names correspond to the ROI IDs provided by Fastsurfer.

features and performing 100 iterations. Within this framework, the RF classifier consistently demonstrated acceptable performance, resulting in an average accuracy with an AUC of 0.917.

To improve the prediction accuracy, we pursued fine-tuning the RF classifier's hyperparameters, which had a positive effect on the results. With these enhancements, the AUC increased to 0.874 with 100 iterations, and we can express our confidence in this outcome with a 95 % confidence interval spanning from 0.822 to 0.912. This demonstrates the robustness and reliability of our predictive model in discerning between AD and MCI, providing valuable insights for clinical applications. Furthermore, the model achieved an accuracy of 0.808, sensitivity of 0.802, and specificity of 0.769, further validating its effectiveness in this task.

3.3. CN vs MCI

As indicated by the findings presented in Table 4, the Random Forest (RF) classifier consistently demonstrated the highest level of accuracy when applied to features selected through the LASSO method. This achievement was particularly notable during 100 iterations, yielding an AUC of 0.879. Furthermore, we can express our confidence in this result with a 95 % confidence interval ranging from 0.747 to 0.911.

In our quest to assess the average accuracy in distinguishing between CN and MCI, we adopted a rank-based approach focusing on the top 80 features, executing 100 iterations for each subset of features. Within this framework, the RF classifier consistently exhibited robust performance, achieving an average accuracy with an AUC of 0.879.

Our analysis further led us to identify the eight most influential features, as depicted in Table 5 based on their impact on accuracy, as visually represented in Fig. 4. Even with this more refined feature set, the model maintained a commendable level of accuracy, resulting in an AUC of 0.778.

We then embarked on the fine-tuning of the RF classifier's hyperparameters, specifically for the top features (eight in total). This fine-tuning effort yielded an average value for the area under the ROC curve (0.79) after 100 iterations. Our confidence in this result is substantiated by a 95 % confidence interval spanning from 0.753 to 0.861. These findings underscore the model's robustness and reliability in

Table 4
(Heatmap) Results of performing nine classifiers GB, RF, DT, GNB, GP, MLP, QDA, AB, and KNN on the top 80 features selected by the eight dimension-reduction methods ANOVA, PCA, Chi2, LASSO, MI, RFA, FI, and RFE to predict CN vs MCI.

`	GB	RF	DT	GNB	GP	MLP	QDA	AB	KNN
ANOVA	0.849	0.878	0.635	0.791	0.693	0.635	0.641	0.847	0.695
PCA	0.862	0.875	0.651	0.771	0.596	0.57	0.625	0.854	0.582
Chi Square	0.798	0.809	0.643	0.779	0.658	0.603	0.583	0.785	0.622
LASSO	0.861	0.879	0.631	0.754	0.692	0.684	0.645	0.858	0.695
MI	0.787	0.793	0.635	0.785	0.649	0.659	0.648	0.767	0.646
RFA	0.821	0.827	0.664	0.791	0.554	0.567	0.665	0.792	0.627
FI	0.802	0.814	0.635	0.775	0.6	0.597	0.676	0.786	0.646
RFE	0.787	0.799	0.638	0.791	0.547	0.631	0.681	0.746	0.68

Table 5
Important Features and ROIs selected by the LASSO method.

CN vs AD						
Feature	ROI	CN		AD		P_Value
		Mean	Std	Mean	Std	
firstorder_90Percentile_1010	isthmuscingulate	1.6166	0.095	1.4252	0.135	1.51E-38
firstorder_Median_1008	inferiorparietal	1.2583	0.08	1.1193	0.14	6.77E-24
glrlm_LongRunEmphasis_17	Hippocampus	51.153	4.959	39.967	7.042	4.51E-45
gldm_DependenceEntropy_2006	entorhinal	3.9792	0.089	4.1798	0.144	9.80E-39
AD vs MCI						
Feature	ROI	AD		MCI		P_Value
		Mean	Std	Mean	Std	
firstorder_90Percentile_1025	precuneus	1.4949	0.136	1.6106	0.108	8.02E-17
firstorder_RootMeanSquared_13	Pallidum	1.1673	0.098	1.0814	0.091	3.29E-16
glrlm_RunLengthNonUniformityNormalized_1009	inferiortemporal	0.1665	0.015	0.1529	0.012	1.59E-18
glrlm_RunVariance_17	Hippocampus	12.474	2.071	14.372	2.249	1.37E-15
firstorder_Median_2022	postcentral	1.2308	0.074	1.187	0.062	4.66E-09
firstorder_90Percentile_2025	precuneus	1.5076	0.146	1.6092	0.108	1.42E-12
CN vs MCI						
Feature	ROI	CN		MCI		P_Value
		Mean	Std	Mean	Std	
firstorder_Maximum_16	Brain Stem	1.4056	0.134	1.4988	0.177	9.51E-09
firstorder_90Percentile_2008	inferiorparietal	1.4771	0.079	1.4344	0.098	3.01E-06
gldm_DependenceVariance_2012	lateralorbitofrontal	22.094	1.001	22.442	1.182	1.87E-03
glszm_ZonePercentage_1022	postcentral	0.0004	3E-04	0.0004	3E-04	7.48E-01
firstorder_Minimum_2035	insula	0.6296	0.075	0.5934	0.081	6.57E-06
shape_Maximum2DDiameterColumn_2020	parstriangularis	29.712	2.342	30.471	2.811	3.97E-03
shape_Sphericity_28	Ventral DC	0.5551	0.015	0.5571	0.016	2.08E-01
glrlm_ShortRunEmphasis_1002	Thalamus	0.2481	0.022	0.2534	0.024	2.21E-02

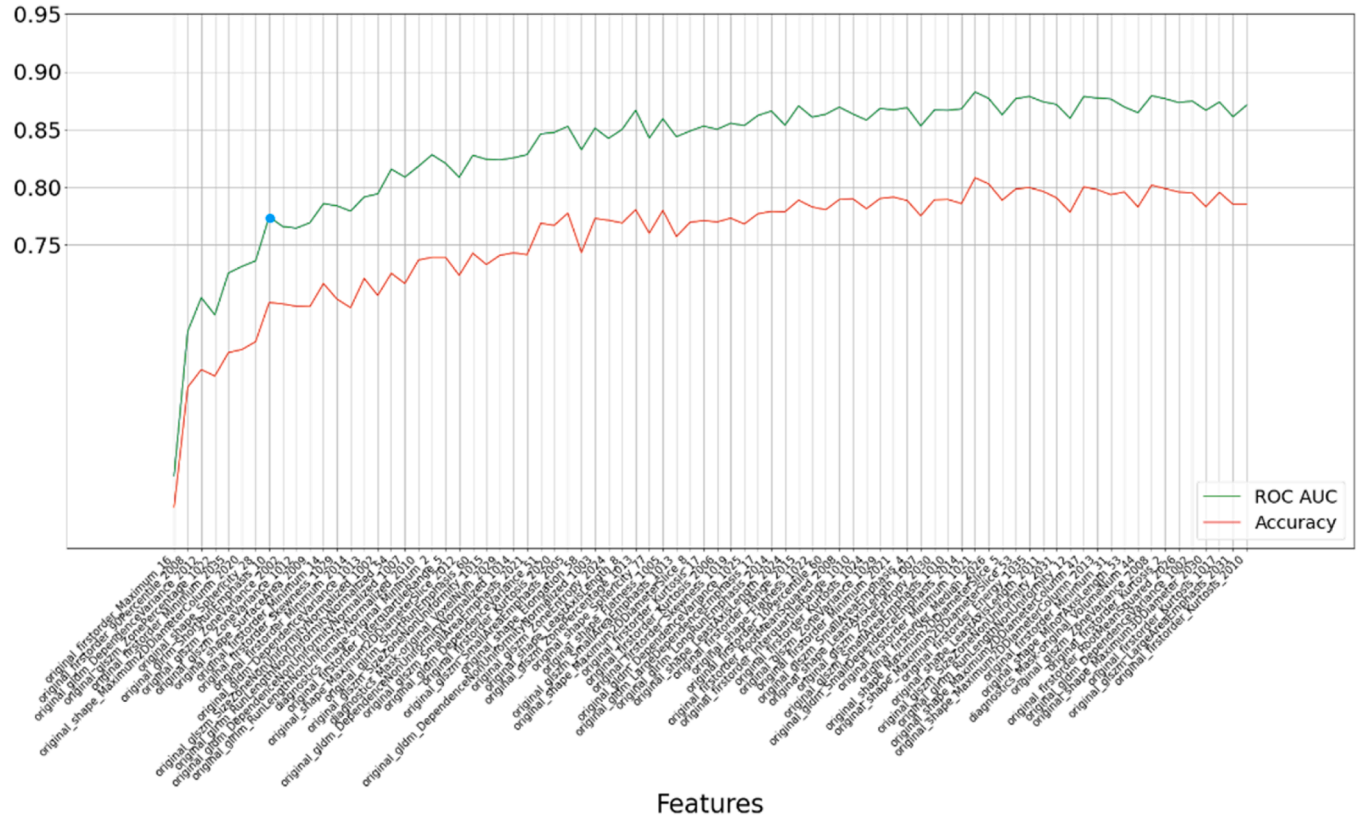

Fig. 4. Rank-based results for each subset of the top 80 most important features selected by the LASSO method. The blue point is the optimal point based on accuracy and feature count. The numbers at the end of the feature names correspond to the ROI IDs provided by Fastsurfer.

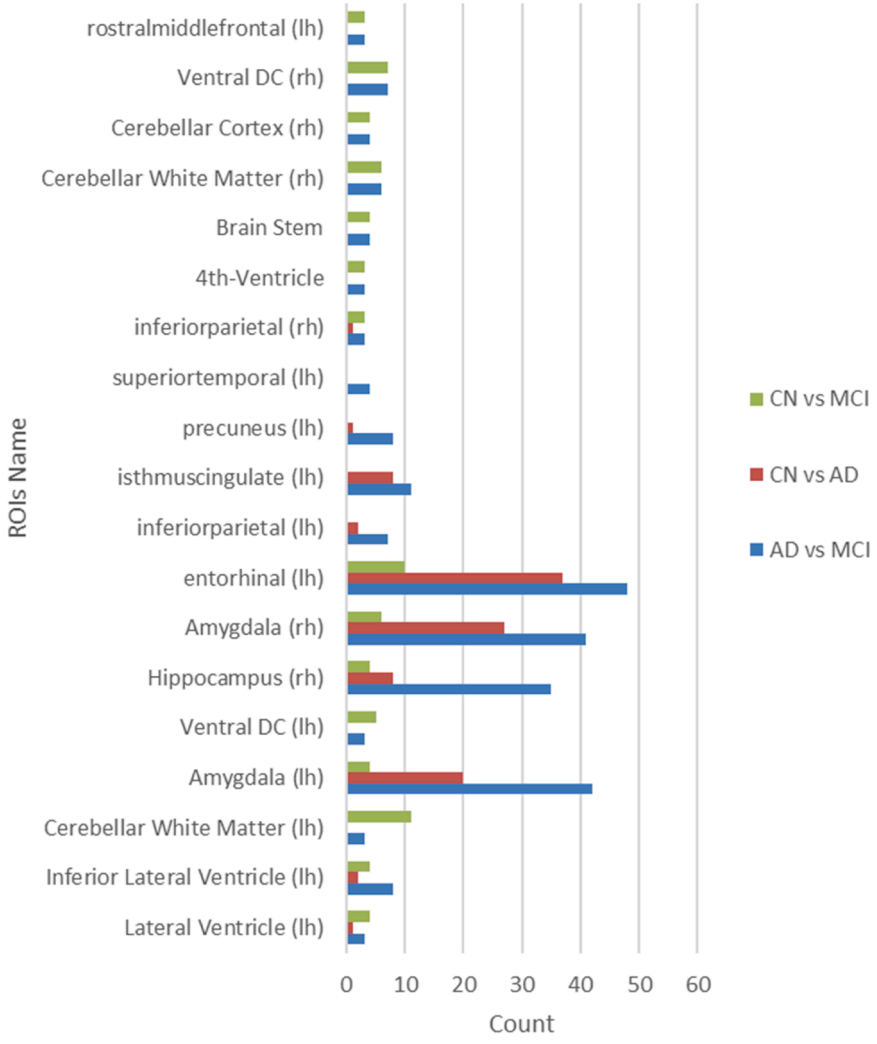

Fig. 5. Common ROIs are frequently selected by eight different feature selection methods.

distinguishing between CN and MCI, carrying significant implications for clinical applications and research. Additionally, the model achieved an accuracy of 0.731, sensitivity of 0.719, and specificity of 0.707, further validating its effectiveness in this task.

To underscore the most efficient Regions of Interest (ROIs) as well as those commonly identified across various prediction scenarios, we present Fig. 5 illustrating the Common ROIs consistently chosen by eight distinct feature selection techniques. Our examination reveals that the amygdala, entorhinal cortex, and hippocampus emerge as the most recurrently utilized regions among the foremost selected features by diverse feature selection methodologies.

Table 6
Comparison of our results with related published studies on the classification of AD.

Author Year	Dataset Size				CN vs AD		CN vs MCI		MCI vs AD		regions	Algorithm	Segmentation	Database/ Modality
	Total	CN	AD	MCI	Acc	AUC	Acc	AUC	Acc	AUC				
Zhigeng Chen 2023	159	53	51	55	0.97	0.98	0.86	0.81	0.85	0.85	hippocampus	Logistic Regression (LR)	SPM12	ADNI / FDG PET-ASL MRI-T1MRI
Alongi, P 2022	43	21	22	–	0.78	–	–	–	–	–	frontal cortex	Discriminant Analysis (DA)	SPM	PET-CT
Yüksel, C 2022	157	132	125	–	–	0.96	–	–	–	–	Whole Brain	Similarity Index + KNN	–	ADNI/FDG PET
Katia M. Poloni 2021	762	302	209	251	0.89	0.95	0.76	0.83	0.69	0.73	AAL (90 Regions) + Land Mark Points	SVM	FSL	ADNI/NAC-IXI sMRI
M. Liu 2020	449	119	97	233	0.88	0.93	0.76	0.78	–	–	Whole Brain	DL (CNN)	–	ADNI/sMRI
Sergey Korolev 2017	231	61	50	120	0.79	0.88	0.63	0.67	0.62	0.61	Whole Brain	DL (CNN)	–	ADNI/sMRI
Proposed Method	549	188	163	198	0.95	0.98	0.81	0.88	0.88	0.91	DKT-atlas (95 regions)	Random Forest (RF)	Fastsurfer	ADNI/FDG PET

4. Discussion

In this study, our primary focus was on diagnosing AD and MCI by developing a radiomics-based platform known as RAB-PET. We also devised a fully automated method to analyze FDG PET brain images in patients with AD and MCI. Early diagnosis of AD is a critical strategy in the context of preventing and treating this debilitating condition. This early diagnosis relies on the measurement of specific characteristics in distinct regions of the human brain, as noted in[40]. Our platform, RAB-PET, provides us with the capability to uncover effective radiomics solutions by exploring nine different classification methods in conjunction with eight diverse feature selection methods, all utilizing FDG PET images. Our approach exhibited a significantly higher level of accuracy compared to recent research efforts detailed in Table 6. This improvement was achieved through the comprehensive exploration of all brain regions, without confining the analysis to any predefined region. Specifically, we achieved an AUC of 0.976 for the AD vs CN, an AUC of 0.917 for the AD vs MCI, and an AUC of 0.879 for MCI vs CN. It's important to acknowledge that direct comparisons with these studies are somewhat constrained due to variations in the datasets and biomarkers used.

For the crucial task of volume analysis, we employed FastSurfer, a novel approach based on deep learning. FastSurfer facilitated the segmentation of the entire brain into 95 distinct regions in less than one minute, drawing upon the DKT atlas. This method offered an efficient alternative to time-consuming brain segmentation techniques like FreeSurfer, Statistical Parametric Mapping (SPM), or FSL, as elaborated in reference[41]. In addition, we harnessed PyRadiomics, which performed the computation of 2D and 3D properties according to the IBSI standard[42,43].

To the best of our knowledge, the developed platform stands out as the first one with the ability to perform radiomics analysis using advanced hardware like CUDA and tensor cores technology for FDG PET images. It's worth emphasizing that FDG PET, recognized for its sensitivity, stands out as the foremost diagnostic imaging method for Alzheimer's Disease, as established by reference[44]. This imaging technique proves to be of value, particularly in the early phases of the disease since metabolic changes occur much earlier than the symptoms.

In the existing literature, several studies have explored the potential of structural magnetic resonance imaging (sMRI) scans for predicting Alzheimer's Disease or Mild Cognitive Impairment, as referenced in[45,46]. It's noteworthy that many recent investigations have adopted a multi-faceted approach, combining various biomarkers, including clinical tests and diverse imaging modalities, to enhance the accuracy of AD and MCI predictions, as indicated by[47]. In contrast, our approach was more streamlined, relying exclusively on FDG PET. We strategically combined sMRI and 18FDG-PET images in the first step to improve segmentation accuracy. We primarily used FDG-PET for analysis. The 17 features extracted from FDG-PET are based on pixel intensity and gray level, providing a detailed view of brain function.

In the investigation outlined in[22], the researchers present a model aimed at predicting AD in patients ($N = 43$) with amyloid positivity. They applied the SPM12 toolbox to define and extract features from four pre-determined regions of interest (ROIs). Subsequently, employing PyRadiomics, they extracted features from these four ROIs. The highest accuracy, reaching 78.05 %, was achieved within a specific ROI, encompassing subregions such as the anterior orbital gyrus (R AOrG), medial orbital gyrus (R MOrG), opercular part of the inferior frontal gyrus (R OpIFG), orbital part of the inferior frontal gyrus (R OrIFG), medial frontal cortex (R MFC), and middle frontal gyrus (R MFG), as well as their corresponding left-sided counterparts. This achievement was made possible through the application of the discriminant analysis (DA) classification method and the incorporation of two higher-order features, specifically original_glcm_MCC and original_glcm_Maximum Probability.

In this investigation[48], scientists focus on the significance of hippocampal imaging for early AD diagnosis, utilizing a multimodal approach. The research employs hybrid PET/MR imaging, incorporating FDG PET, T1 MRI, and ASL-MRI to capture glucose metabolism changes in the hippocampus. They predicted distinct stages of AD by leveraging a cohort comprising 51 CE patients, 55 individuals with MCI, and 53 older participants with normal cognitive function (NC). The researchers employed predefined regions of interest (ROIs) based on the hippocampus template provided by the Johns Hopkins Department of Radiology, manually delineated on the MRI template. Subsequently, features were extracted using PyRadiomics, and dimensionality reduction was accomplished through the LASSO method. The logistic regression (LR) models yielded favorable outcomes with Area Under the Curve (AUC) values of 0.98 % for distinguishing between normal cognition and AD (CN vs AD), 0.81 for CN vs MCI, and 0.85 for MCI vs AD.

In this investigation[49], researchers explored hippocampal asymmetry by considering differences between the left and right hemispheres. They introduced a novel asymmetry index, utilizing the first four statistical moments (mean, variance, skewness, and kurtosis) calculated from the magnitude map of the oriented log-Gabor filter response within the hippocampus region. Subsequently, an assessment for asymmetry was conducted using the one-way analysis of variance (ANOVA) test, and the attributes exhibiting statistically significant mean differences among the classes (CN, MCI, and AD) were selected. These selected attributes were then utilized in classification by Support Vector Regression (SVR). The results demonstrated meaningful distinctions among classes, with achieved area under the curve (AUC) values of 0.76 for CN vs MCI and 0.9 for CN vs AD, showcasing the effectiveness of the proposed asymmetry-based approach.

In this study, after extracting features from FDG PET scans, we took measures to optimize computation time. This involved preprocessing the features and eliminating the unnecessary features by eliminating constant, quasi-constant, and duplicated features. This reduction in feature set size aimed to enhance efficiency while maintaining the predictive power of our approach. Furthermore, for the sake of result interpretability, we went a step further by selecting the most vital features based on their contribution to accuracy and feature count. For CN vs. AD, we retained 'n=4′ critical features, for AD vs. MCI, 'n=6′, and for CN vs. MCI, 'n=8′. This step not only enhanced the practical utility of our predictions but also facilitated a better understanding of the underlying factors driving our diagnostic capabilities in different scenarios.

In our study, we discovered that various prediction models exhibit a preference for different brain regions and features. However, in our quest to identify shared regions among these distinct prediction scenarios, we conducted an extensive analysis. This analysis revealed a consistent finding: the amygdala, entorhinal cortex, and hippocampus consistently emerged as pivotal regions across all stages of Alzheimer's disease.

These three brain regions, known for their roles in memory and cognitive function, demonstrated their enduring significance in our predictive model. This finding suggests that, regardless of the specific predictive task or feature selection method, the amygdala, entorhinal cortex, and hippocampus remain robust markers that hold vital relevance throughout the progression of Alzheimer's disease. This insight has the potential to enhance the accuracy and consistency of diagnostic and predictive models, ultimately contributing to our understanding and management of this disease.

Furthermore, an additional discovery from our study is the identification of four frequently employed features (namely, gldm_DependenceEntropy, shape_SurfaceVolumeRatio, glrlm_RunPercentage, glrlm_LongRunEmphasis) by eight distinct feature selection methods. These features were consistently recognized as the most critical in predicting AD within three specific Regions of Interest (ROIs): the amygdala, entorhinal cortex, and hippocampus (as depicted in Fig 5). GLDM measures the degree of randomness or non-uniformity in an image. gldm_DependenceEntropy: This feature measures texture complexity, potentially reflecting alterations in tissue microstructure due to

neurodegeneration in AD and MCI. In other words, a larger value of a textural feature extracted from GLDM corresponds to a heterogeneous and irregular spatial distribution, with a series of complex correlation structures between the voxels[50].

Textural features such as glrlm_RunPercentage and glrlm_LongRunEmphasis were employed to detect structural and morphological changes within brain regions, aiding in the diagnosis and comprehension of cognitive and behavioral impairments in individuals with AD and MCI[51,52]. These features play a pivotal role in delineating subtle alterations in brain tissue, contributing valuable insights into the progression of neurodegenerative conditions and facilitating more targeted interventions for affected patients.

Shape_SurfaceVolumeRatio: This feature acts as a sensitive gauge for morphological alterations within brain regions, particularly those susceptible to neurodegeneration in AD and MCI like the hippocampus. An elevated ratio signifies a shrinking tissue volume relative to the remaining surface area, potentially reflecting cellular loss and atrophy. This phenomenon is most commonly observed in the hippocampus, a key structure for memory and navigation, and often worsens with the progression of AD.

The rationale is that an optimal radiomics study that automatically generates the significant regions and features can give us both higher accuracy and more information on the potential biological mechanisms of the disease. This may have also an effect on the ease of interpretation of the results.

This research illustrates how radiomic analysis can confirm both biological theories and clinical observations. Based on recent clinical investigations involving Alzheimer's Disease patients, it can be concluded that these three ROIs are the most affected parts of the brain related to AD. A recent study introduced the entorhinal, amygdala, and parahippocampal regions as early tau-deposited regions of temporal meta-ROI, which can assist in the early diagnosis of AD disease[53]. In addition, according to the report of the National Institute on Aging (NIH), Alzheimer's disease typically destroys neurons and their connections in parts of the brain involved in memory, including the entorhinal cortex and hippocampus. It later affects areas in the cerebral cortex responsible for language, reasoning, and social behavior[54].

Another contribution of this study is to show how the classification and the feature reduction methods affect the results. We investigated nine classification methods on the eight different feature selection methods to find the best combination of feature selection and classification methods. We found that LASSO is a well-performing feature selection method with the RF classifier in FDG PET images.

This study has some limitations. Despite the promising results of radiomics in various fields of medicine and its potential application in precision medicine[55], deep exploration, refinement, standardization, and validation are still required for application in clinical practice[56]. Future work is needed to perform these studies. Therefore, validating the proposed models by further multicenter studies is a necessary step that requires the provision of a comprehensive and standard solution to verify them for use in clinical practice. Moreover, many factors influence the outcomes of the radiomics approach, and therefore this field relies on the performance of different methods, such as segmentation, feature extraction, and classification[57].

Our study confirms that FDG PET can be an important biomarker for AD in comparison with recent studies as shown in Table 6. We believe that the predictive performance of the proposed solution can be improved by extending the dataset size or combining it with other existing datasets. In future work, the same platform and methodology can be tested to detect other neurological diseases or to predict other quantitative characteristics of AD[58].

5. Conclusion

In summary, we developed the RAB-PET platform which offers an efficient and accurate solution for the radiomic analysis of brain FDG PET images. Testing on AD and MCI patients has shown its potential for reliable AD diagnosis and identification of its stages, accomplished with minimal computational time. It also helps the computational identification of the few most important regions and features without any prior assumptions. This improves both accuracy and explainability. Furthermore, it may contribute to the understanding of the pathology. Future work will concentrate on using the same platform and methodology to detect other neurological diseases or to predict other quantitative characteristics of AD[58].

Ethical approval

Funding

This research received funding from the Bogazici University Research Fund (BAP) under project code 19,774. The financial support played a crucial role in conducting the experiments and analyzing the data.

Use of patient data

The study does not use unpublished patient data and is a retrospective study. Data exclusively came from publicly available online sources, specifically the Alzheimer's Disease Neuroimaging Initiative (ADNI).

Consent to participate

No participant's consent was required as the research solely utilized publicly available online data from ADNI.

Consent to publish

Acknowledging the use of the ADNI dataset, this research respects ADNI data usage terms. As the data is de-identified and publicly available, individual consent for publication was unnecessary.

Animal experiments

The study does not include any animal experiments.

Clinical trial

The study is not a clinical trial; it involved an analysis of online data for the early detection of Alzheimer's disease.

Case report

The study is not a case report.

References to tables and figures

Tables and figures are referenced in the paper.

Authorship confirmation

All authors listed in the submission are the same as those whose names appear on the full-text paper.

CRediT authorship contribution statement

Ramin Rasi: Writing – original draft, Methodology, Formal analysis, Data curation. **Albert Guvenis:** Writing – review & editing, Methodology, Funding acquisition, Data curation, Conceptualization.

Declaration of competing interest

A statement regarding conflicts of interest has been made, confirming that there are no conflicts associated with this research or submission.

Acknowledgments

We gratefully acknowledge the financial support provided by the Bogazici University Research Fund (BAP) for this research under project code 19774. Their support was instrumental in carrying out the experiments and analyzing the data.

Data collection and sharing for this project was funded by the Alzheimer's Disease Neuroimaging Initiative (ADNI) (National Institutes of Health Grant U01 AG024904) and DOD ADNI (Department of Defense award number W81XWH-12-2-0012). ADNI is funded by the National Institute on Aging, the National Institute of Biomedical Imaging and Bioengineering, and through generous contributions from the following: AbbVie, Alzheimer's Association; Alzheimer's Drug Discovery Foundation; Araclon Biotech; BioClinica, Inc.; Biogen; Bristol-Myers Squibb Company; CereSpir, Inc.; Cogstate; Eisai Inc.; Elan Pharmaceuticals, Inc.; Eli Lilly and Company; EuroImmun; F. Hoffmann-La Roche Ltd and its affiliated company Genentech, Inc.; Fujirebio; GE Healthcare; IXICO Ltd.; Janssen Alzheimer Immunotherapy Research & Development, LLC.; Johnson & Johnson Pharmaceutical Research & Development LLC.; Lumosity; Lundbeck; Merck & Co., Inc.; Meso Scale Diagnostics, LLC.; NeuroRx Research; Neurotrack Technologies; Novartis Pharmaceuticals Corporation; Pfizer Inc.; Piramal Imaging; Servier; Takeda Pharmaceutical Company; and Transition Therapeutics. The Canadian Institutes of Health Research is providing funds to support ADNI clinical sites in Canada. Private sector contributions are facilitated by the Foundation for the National Institutes of Health (www.fnih.org). The grantee organization is the Northern California Institute for Research and Education, and the study is coordinated by the Alzheimer's Therapeutic Research Institute at the University of Southern California. ADNI data are disseminated by the Laboratory for Neuro Imaging at the University of Southern California.

References

[1] 2020 Alzheimer's disease facts and figures. *Alzheimer's and Dementia* 16, 391–460 (2020).
[2] *World Alzheimer Report 2023 Reducing Dementia Risk: never Too Early, Never Too Late*. https://www.alz.org/.
[3] L. Younes, et al., Identifying changepoints in biomarkers during the preclinical phase of Alzheimer's disease, Front Aging Neurosci 11 (2019).
[4] J.D. Grill, C.G. Cox, K. Harkins, J. Karlawish, Reactions to learning a 'not elevated' amyloid PET result in a preclinical Alzheimer's disease trial, Alzheimers Res Ther 10 (2018).
[5] A. Revathi, et al., Early Detection of Cognitive Decline Using Machine Learning Algorithm and Cognitive Ability Test, Security and Communication Networks 2022 (2022) 1–13.
[6] R.K. Verma, et al., An Insight into the Role of Artificial Intelligence in the Early Diagnosis of Alzheimer's Disease, CNS Neurol Disord Drug Targets 21 (2022) 901–912.
[7] J. Guiot, et al., A review in radiomics: making personalized medicine a reality via routine imaging, Med Res Rev 42 (2022) 426–440.
[8] Chen, Z. et al. Early Diagnosis of Alzheimer's Disease using Multiparametric Hippocampal Signatures with 18F-FDG PET/MR Radiomics. Preprint at (2023).
[9] J. Hu, et al., Diagnostic performance of magnetic resonance imaging–based machine learning in Alzheimer's disease detection: a meta-analysis, Neuroradiology 65 (2023) 513–527.
[10] D.W. Kim, H.Y. Jang, K.W. Kim, Y. Shin, S.H. Park, Design Characteristics of Studies Reporting the Performance of Artificial Intelligence Algorithms for Diagnostic Analysis of Medical Images: results from Recently Published Papers, Korean J Radiol 20 (2019) 405.
[11] J. Peng, et al., 18F-FDG-PET Radiomics Based on White Matter Predicts The Progression of Mild Cognitive Impairment to Alzheimer Disease: a Machine Learning Study, Acad Radiol 30 (2023) 1874–1884.
[12] J.L. Shaffer, et al., Predicting Cognitive Decline in Subjects at Risk for Alzheimer Disease by Using Combined Cerebrospinal Fluid, MR Imaging, and PET Biomarkers, Radiology 266 (2013) 583–591.
[13] P. Linardatos, V. Papastefanopoulos, S. Kotsiantis, Explainable ai: a review of machine learning interpretability methods, Entropy 23 (2020) 18.
[14] J.D. Rudie, A.M. Rauschecker, R.N. Bryan, C. Davatzikos, S. Mohan, Emerging Applications of Artificial Intelligence in Neuro-Oncology, Radiology 290 (2019) 607–618.
[15] R. Rasi, A. Guvenis, Predicting amyloid positivity from FDG-PET images using radiomics: a parsimonious model, Comput Methods Programs Biomed 247 (2024) 108098.
[16] C. Yuksel, R. Rasi, A. Guvenis, A New Method for Diagnosing Alzheimer's Disease and Monitoring Its Severity Using FDG-PET, in: 2022 Medical Technologies Congress (TIPTEKNO), IEEE, 2022, pp. 1–4, https://doi.org/10.1109/TIPTEKNO56568.2022.9960196.
[17] D. Shamonin, Fast parallel image registration on CPU and GPU for diagnostic classification of Alzheimer's disease, Front Neuroinform 7 (2013).
[18] P. Valero-Lara, Multi-GPU acceleration of DARTEL (early detection of Alzheimer), in: 2014 IEEE International Conference on Cluster Computing (CLUSTER), IEEE, 2014, pp. 346–354, https://doi.org/10.1109/CLUSTER.2014.6968783.
[19] A.P. Apte, et al., Technical Note: extension of CERR for computational radiomics: a comprehensive MATLAB platform for reproducible radiomics research, Med Phys 45 (2018) 3713–3720.
[20] Z. Zhou, et al., A new machine learning based user-friendly software platform for automatic radiomics modeling and analysis, in: 2021 43rd Annual International Conference of the IEEE Engineering in Medicine & Biology Society (EMBC), IEEE, 2021, pp. 2810–2814, https://doi.org/10.1109/EMBC46164.2021.9630472.
[21] B.FreeSurfer Fischl, Neuroimage 62 (2012) 774–781.
[22] P. Alongi, et al., Radiomics analysis of brain [18F] FDG PET/CT to predict Alzheimer's disease in patients with amyloid PET positivity: a preliminary report on the application of SPM cortical segmentation, pyradiomics and machine-learning analysis, Diagnostics 12 (2022) 933.
[23] W.J. Jagust, et al., The Alzheimer's Disease Neuroimaging Initiative 2 PET Core: 2015, Alzheimer's Dementia 11 (2015) 757–771.
[24] J.J.M. van Griethuysen, et al., Computational Radiomics System to Decode the Radiographic Phenotype, Cancer Res 77 (2017) e104–e107.
[25] P. Ray, S.S. Reddy, T. Banerjee, Various dimension reduction techniques for high dimensional data analysis: a review, Artif Intell Rev 54 (2021) 3473–3515.
[26] M.A. Salam, A. Taher, M. Samy, K. Mohamed, The Effect of Different Dimensionality Reduction Techniques on Machine Learning Overfitting Problem, International Journal of Advanced Computer Science and Applications 12 (2021).
[27] A. Jović, K. Brkić, N. Bogunović, A review of feature selection methods with applications, in: 2015 38th international convention on information and communication technology, electronics and microelectronics (MIPRO), 2015, pp. 1200–1205.
[28] R. Massafra, et al., Radiomic feature reduction approach to predict breast cancer by contrast-enhanced spectral mammography images, Diagnostics 11 (2021) 684.
[29] M.E. Mayerhoefer, et al., Introduction to radiomics, Journal of Nuclear Medicine 61 (2020) 488–495.
[30] Z. Shu, et al., MRI-based Radiomics nomogram to detect primary rectal cancer with synchronous liver metastases, Sci Rep 9 (2019) 3374.
[31] R. Muthukrishnan, R. Rohini, LASSO: a feature selection technique in predictive modeling for machine learning, in: 2016 IEEE international conference on advances in computer applications (ICACA), 2016, pp. 18–20.
[32] A.D. Henriques, A.L. Benedet, E.F. Camargos, P. Rosa-Neto, O.T. Nóbrega, Fluid and imaging biomarkers for Alzheimer's disease: where we stand and where to head to, Exp Gerontol 107 (2018) 169–177.
[33] P. Probst, A.-L. Boulesteix, B. Bischl, Tunability: importance of hyperparameters of machine learning algorithms, The Journal of Machine Learning Research 20 (2019) 1934–1965.
[34] E. Elgeldawi, A. Sayed, A.R. Galal, A.M. Zaki, Hyperparameter Tuning for Machine Learning Algorithms Used for Arabic Sentiment Analysis, Informatics 8 (2021) 79.
[35] M. Bogowicz, et al., Post-radiochemotherapy PET radiomics in head and neck cancer–the influence of radiomics implementation on the reproducibility of local control tumor models, Radiotherapy and Oncology 125 (2017) 385–391.
[36] A. Zwanenburg, et al., The image biomarker standardization initiative: standardized quantitative radiomics for high-throughput image-based phenotyping, Radiology 295 (2020) 328–338.
[37] Rasi Ramin & Guvenis Albert. RAB-PET. (2023) doi:10.5281/zenodo.7859694.
[38] X. Ying, An Overview of Overfitting and its Solutions, J Phys Conf Ser 1168 (2019) 022022.
[39] P. Ray, S.S. Reddy, T. Banerjee, Various dimension reduction techniques for high dimensional data analysis: a review, Artif Intell Rev 54 (2021) 3473–3515.
[40] A.M. Franceschi, D. Franceschi, Hybrid PET/MR Neuroimaging: A Comprehensive Approach, Springer Nature, 2021.
[41] L. Palumbo, et al., Evaluation of the intra- and inter-method agreement of brain MRI segmentation software packages: a comparison between SPM12 and FreeSurfer v6.0, Physica Medica 64 (2019) 261–272.
[42] A. Zwanenburg, et al., The image biomarker standardization initiative: standardized quantitative radiomics for high-throughput image-based phenotyping, Radiology 295 (2020) 328–338.
[43] M. Bogowicz, et al., Post-radiochemotherapy PET radiomics in head and neck cancer–the influence of radiomics implementation on the reproducibility of local control tumor models, Radiotherapy and Oncology 125 (2017) 385–391.
[44] A. Wabik, et al., Comparison of dynamic susceptibility contrast enhanced MR and FDG-PET brain studies in patients with Alzheimer's disease and amnestic mild cognitive impairment, J Transl Med 20 (2022) 1–14.
[45] S. Basaia, et al., Automated classification of Alzheimer's disease and mild cognitive impairment using a single MRI and deep neural networks, Neuroimage Clin 21 (2019) 101645.

[46] A.H. Syaifullah, et al., Machine learning for diagnosis of AD and prediction of MCI progression from brain MRI using brain anatomical analysis using diffeomorphic deformation, Front Neurol 11 (2021) 576029.
[47] Y. Gupta, R.K. Lama, G.-R. Kwon, A.D.N. Initiative, Prediction and classification of Alzheimer's disease based on combined features from apolipoprotein-E genotype, cerebrospinal fluid, MR, and FDG-PET imaging biomarkers, Front Comput Neurosci 13 (2019) 72.
[48] Chen, Z. et al. Early Diagnosis of Alzheimer's Disease using Multiparametric Hippocampal Signatures with 18F-FDG PET/MR Radiomics. Preprint at (2023).
[49] K.M. Poloni, et al., Brain MR image classification for Alzheimer's disease diagnosis using structural hippocampal asymmetrical attributes from directional 3-D log-Gabor filter responses, Neurocomputing 419 (2021) 126–135.
[50] J. Li, et al., Correlation of [18F]florbetaben textural features and age of onset of Alzheimer's disease: a principal components analysis approach, EJNMMI Res 11 (2021) 40.
[51] Q. Feng, et al., Corpus Callosum Radiomics-Based Classification Model in Alzheimer's Disease: a Case-Control Study, Front Neurol 9 (2018).
[52] F. Feng, et al., Radiomic Features of Hippocampal Subregions in Alzheimer's Disease and Amnestic Mild Cognitive Impairment, Front Aging Neurosci 10 (2018).
[53] Y. Cai, et al., Initial levels of β-amyloid and tau deposition have distinct effects on longitudinal tau accumulation in Alzheimer's disease, Alzheimers Res Ther 15 (2023) 30.
[54] 2023 Alzheimer's disease facts and figures, Alzheimer's & Dementia 19 (2023) 1598–1695.
[55] A.A. Ardakani, N.J. Bureau, E.J. Ciaccio, U.R. Acharya, Interpretation of radiomics features–a pictorial review, Comput Methods Programs Biomed 215 (2022) 106609.
[56] A.-N. Frix, et al., Radiomics in lung diseases imaging: state-of-the-art for clinicians, J Pers Med 11 (2021) 602.
[57] S.S.F. Yip, H.J.W.L Aerts, Applications and limitations of radiomics, Phys Med Biol 61 (2016) R150–R166.
[58] J. Zhang, Y. Gao, Y. Gao, B.C. Munsell, D. Shen, Detecting anatomical landmarks for fast Alzheimer's disease diagnosis, IEEE Trans Med Imaging 35 (2016) 2524–2533.